Dynamical Invigoration of Electrified Storms

Dipjyoti Mudiar[1], Earle Williams[2], S. D. Pawar[1], Anupam Hazra[1], Rama Krishna Karumuri[3], V. Gopalakrishnana[1], Mahen Konwar[1], Rakesh Ghosh[1], Manoj A Domkawale[1], Kaustav Chakravarty[1], M. K. Srivastava[4], and B N Goswami[5]

[1]Indian Institute of Tropical Meteorology, Ministry of Earth Sciences, Pune, India, 411008

[2]Massachusetts Institute of Technology, Cambridge, MA USA

[3]King Abdullah University of Science and Technology, Thuwal, Saudi Arabia

[4]Banaras Hindu University, Varanasi, India 221005

[5]Cotton University, Guwahati, India 781001

Abstract

The recent emergence of compelling evidence (*Mudiar et al*., 2018, 2021a 2021b) regarding a significant impact of cloud electrification on rain microphysical processes raises curiosity on the potential dynamical implications of cloud electrification. In this study, the consequence of cloud electrification has been explored from a perspective of interaction between cloud microphysics and dynamics using observational data and numerical models in a tropical condition. It is shown that the strongly electrified (SE) clouds exhibit a reduced value of rain intercept parameter, N_0 relative to the weakly electrified (WE) counterpart facilitated by the in-cloud electric field. This process results in a reduction in rain evaporation rate in the warm phase of the cloud, thereby enhancing the surface rain intensity. From a dynamical perspective, the reduced rain evaporation rate gives positive feedback to storm energetics by reducing latent cooling. The reduced latent cooling delays the downdraft thereby facilitating an invigoration of convection. This electrically induced invigoration is termed '*Dynamical Invigoration of Electrified Storms*'.

1. Introduction

Clouds are manifestations of uplift of air either by convection, orography or by waves in the atmosphere. Convective overturning enables the atmosphere to release the stored potential energy by converting it to the kinetic energy of air motion. The cloud droplets resulting from the convection transformed into raindrops by different microphysical processes and produce surface precipitation as the end product which drives the Earth's hydrological cycle. The microphysical processes that convert the cloud droplets to raindrops differ depending upon the type and stages of convection (active and decaying). For example, in convective precipitation with a stronger updraft, precipitation arises from the collection of cloud droplets in the warm phase of the cloud and by freezing, riming and aggregation of snow in the mixed-phase in the presence of substantial supercooled liquid water (*Houze,* 1997). When the updraft weakens in the decaying stage of a storm, the growth of precipitation particles primarily happens through vapor diffusion and aggregation in the mixed-phase region of the cloud (*Houze,* 1997), which is known as stratiform precipitation. Once the precipitation particles form, they evolve through different microphysical processes such as collision, coalescence, breakup, evaporation and sublimation. The prevailing microphysical processes determine the raindrop size distribution, RDSD (*Konwar et al.,* 2014) and hence the total amount of rain received at the surface (*Morrison et al*., 2009, 2012). Hence a proper understanding of the cloud microphysics that impact the rain amount and intensity is very important.

One factor that is external to the convection, but can feedback on the convection and hence on the rain amount and its intensity is the aerosol size and its number concentration. Numerous high impact investigations can be found in the literature in support of this scenario (*Rosenfeld*, 1999; *Tao et al*., 2012; *Khain et al*., 2005; *Rosenfeld*, 2008 and reference therein). The other factor (also external to convection) that could potentially impact the rain formation mechanisms is cloud electrification (*Pruppacher and Klett*, 1996 and references therein). Cloud

electrification and consequent lightning is the visual manifestation of the interaction between cloud convection and hydrometeors. The lightning-producing clouds exhibit vertical electric fields reaching 400 kVm^{-1} (Winn et al,. 1974) with hydrometeor charge up to ±250 pC (*Christian et al*., 1980). Hence, this fraction of clouds can be termed as strongly electrified (SE). In lightning-producing clouds, different charging mechanisms involving ice phase microphysical processes mediated by stronger vertical air velocity produces the required electric field for electrical breakdown. The primary charging mechanism is the non-inductive charging where collision between smaller ice crystals and larger size graupels is considered as the primary process (*Takahasi*, 1978; *Bruning et al*., 2007; *Bruning et al*., 2010).

Although the common initiator of both precipitation and lightning is cloud convection, both show different sensitivity to the convective intensity (*Williams*, 2005). While lightning remains associated with deeper and stronger updraft than does precipitation, numerous observations reported that both these observables remain well correlated during tropical thunderstorms (*Piepgrass et al.* 1983, *Mudiar et al*., 2021a, Choudhury et al., 2021). One potential explanation of this observed correlation is the substantial contribution of precipitation to storm electrification and consequent lightning production (*Williams and Lhermitte*, 1983). They reported that the gravitational energy associated with falling precipitation could substantially contribute to the electrical energy of a lightning discharge. However, not much attention has been paid to understanding the reverse feedback process, i.e., the impact of electrification on precipitation formation despite having extensive evidence for the same both from laboratory and numerical studies (see *Pruppacher and Klett*, 1996). Recent observational studies have shown that rain microphysical processes in strongly electrified (SE) clouds are distinctly different from those in weakly electrified (WE) clouds, which is conventionally attributed to the vigorous ice factory in SE clouds (Mattos et al., 2016). Weakly electrified clouds (exhibiting weaker updraft intensity) are often warm clouds that do not strongly penetrate the freezing level. The SE cloud produces a larger number of bigger raindrops relative to the WE counterpart. The presence of larger raindrops in SE clouds can be attributed to three characteristic microphysical processes as discussed below.

(a) Melting of larger graupel/hail particles

This is the conventional hypothesis to explain the presence of larger raindrops in lightning-producing clouds (SE). The coexistence of a larger concentration of smaller ice particles and bigger graupels along with supercooled raindrops in the mixed-phase region of cloud are considered essential for charge separation and consequent electrification (*Takahashi*, 1978*; Mattos et al*., 2016). Numerous dual-pol radar observations indicate large radar reflectivity (Z>30 dBZ) in the mixed-phase region, indicating the presence of larger graupel/hail particles and aggregates (*Mattos et al.*, 2016, *Carey and Rutledge*, 2000). The more vigorous the storm ice factory, the stronger will be the electrification. When these particles drift downward, they produce bigger raindrops below the melting layer upon melting. However, while drifting down below the melting level, the raindrop evolves through collision, coalescence, breakup and evaporation (readers are referred to *Konwar et al*., 2014 and Raut et al., 2021 for a detailed description on the vertical evolution of drops size).

(b) Electric fields induce coalescence of raindrops below the melting layer

The in-cloud electric field and surface charge can also enhance the collision-coalescence growth of raindrops *(Mudiar et al*., 2021b and references therein). In the presence of stronger electrical environments typical of lightning-producing clouds, the enhanced collision-coalescence of raindrops facilitated by cloud electric field (*Pruppacher and Klett*, 1996 and references therein) below the melting layer can broaden the RDSD towards the larger drop sizes(*Mudiar et al*., 2018). It has been observed that in a SE cloud, the electrically induced coalescence of raindrops increases the number concentration of bigger raindrops, thereby reducing the number of smaller drops (*Mudiar et al*., 2021b).

(c) Lightning-induced precipitation formation

Thunderstorms are known to exhibit a close association between lightning rate and rainfall rate (Piepgrass et al., 1982; Price and Federmesser 2006, Mudiar et al., 2021a). The pre-discharge updraft levitation of precipitation particles is known to occur in the so-called balance level situated at 6-7km MSL height (Lhermitte and Williams, 1985). It may be noted here that the pre-discharge levitation of precipitation particles may be either kind: aerodynamic levitation or electrical levitation. Lightning reduces the pre-discharge electric force. The reduction of electrical forces after the lightning allows the precipitation particles to drift downward in the

form of graupel and small hail. The melting of these particles produces numerous large as well as small drops below the melting layer, thereby enhancing the surface rainfall known as raingush. This raingush may occur from the collapse of aerodynamic as well as electrical levitation of particles. A recent study by Mudiar et al., (2021a) suggests that lightning can modify the size of raindrops by depositing ions near the channel. The attachment of these ions to the raindrops make them electrified. The electrified drops coalesce efficiently to produce larger raindrops and thereby enhance the rain rate. For a detailed explanation of this process, readers are referred to Mudiar et al. (2021a).

The simulation of precipitation using Numerical Weather Prediction (NWP) models has been improved significantly at synoptic and mesoscales over the years (Boer et al., 2014). However, large mean absolute errors (MAE~10 to 14) for the heavy rain intensity (>10mm) still persist in the quantitative precipitation forecast (QPF)(*Giannaros et al*., 2015). One potential source of this large MAE may be inaccurate information on the RDSD. An accurate information on the RDSD is considered important for understanding precipitation physics and improving the microphysics parameterization in NWP models (*Steiner et al*., 2004). On the other hand, it has been reported that a substantial amount of the rainfall (~57%) in the latitude belt of 30^{o} N–30^{o} S could be attributed to Mesoscale Convective Systems (MCS) (*Virts and Houze,* 2015). The convective and the stratiform regimes of MCS over the Maritime Continent remain associated with strong electrification (*Williams et al*., 2010). This suggests that a large fraction of tropical precipitation comes from strongly electrified clouds where electrical forces can affect the rain microphysical processes (Sun et al., 2018). So, an effective parameterization of the electrical effect in the physics schemes of weather/climate models can provide a potential opportunity to improve the representation of this fraction of cloud in the NWP models. Also, many studies suggest that the prevailing microphysical processes can strongly impact the in-cloud dynamics (e.g. updrafts and downdrafts) (*Grabowski*, 2015; *Rosenfeld,* 2008; *Morrison et al*., 2009; *Hazra et al.,* 2013). However, how the feedback between the anomalous dynamics and microphysics influences the resultant precipitation is not known. As the electrical impact on the rain microphysical processes is now reasonably well established (*Mudiar et al*., 2018, 2021a, 2021b, 2022), feedback to the dynamical features of storms from the electrically modified microphysical processes can be expected in a SE tropical cloud systems.

With this background, in this paper we investigate a NWP model's sensitivity to electrically modified RDSD parameters and a possible feedback mechanism of cloud electrification to the dynamical parameters of storms. First, the clouds are electrically distinguished based on observational data sets. The microphysical properties of both types of cloud are investigated and some statistics have been derived for the RDSD parameters in SE rain events. The second half of the paper is dedicated to a numerical experiment using a numerical weather model. Results from the simulation experiment have been presented in order to investigate the sensitivity of model-simulated cloud microphysical and dynamics parameters to electrically-modified RDSDs. In the discussion section, some possible mechanisms of storm invigoration have been discussed. The main conclusions of the paper have been summarized in the conclusion section.

2. Data and Methodology

The results and interpretations presented in this paper pertain to analysis of both observational data sets and numerical modeling. Some of the meteorological observations presented here were carried out at the High Altitude Cloud Physics Laboratory (HACPL), Mahabaleshwar, (India; 17.92 N, 73.66 E). The electrical parameters of storms, such as surface-electric field were measured at the Atmospheric Electricity Observatory (AEO) at Pune, (India; 18.53N, 73.80E). The distance of the AEO from the HACPL is around 100 km (see Figure 1a). The topographical features and climatology of both the observation sites have been extensively discussed in *Mudiar at el*. (2021a). The measurements of the RDSD parameters reported in this study are carried out with a surface-based Joss-Waldvogel disdrometer (JWD) located at the HACPL and a laser optical Particle Size and Velocity (PARSIVEL) disdrometer, located at the AEO. The Doppler spectra obtained from a microrain radar (MRR) installed at the HACPL have been used to study the vertical profiles of radar reflectivity and RDSD. There are numerous papers describing the usefulness and limitations of these three measuring instruments (*Joss and Waldvogel*, 1967; *Peters et al*.,2005; *Löffler-Mang and Joss*,2000; *Konwar et al*,2014; *Mudiar et al*., 2018, 2021a). Hence, with a view to brevity, we will abstain from discussing them again here. However, when necessary the data curation from the instruments and the related measurements errors will be discussed.

All the simulation experiments reported in the current study are performed using the Advanced Weather Research and Forecasting (WRF-ARW) model version 3.9.1. The WRF model is developed by the National Center for Atmospheric Research (NCAR). It is a fully compressible, non-hydrostatic, terrain-following 3D mesoscale model. Two kinds of simulation experiments are carried out: a set of idealized simulations and a set of observed case simulations. The model set up and model initialization for the idealized simulations are extensively discussed in section 3.5. The simulations for the observed cases are carried out considering four nested domain (d01, d02, d03, d04) configurations. The four domains are configured with a horizontal grid spacing of 27km, 9km, 3km and 1km, respectively. Figure 1b depicts the geographical coverage of the model domain. The domain d04 (innermost) is centered on the HACPL. For the observed case simulations, the initial and boundary conditions are provided from 6 hourly final operational global analysis (NCEP-FNL) data. The NCEP-FNL data is available with $1^o \times 1^o$ horizontal resolution. For long wave radiation, the Rapid Radiative Transfer Model (RRTM) has been used, as discussed in *Mlawer et al*. (1997). For short wave radiation, the Dudhia scheme (*Dudhia*, 1989) has been used. While the two innermost cloud-resolving domains (3rd and 4th) are treated with explicit convection, the Betts Miller Janjic (BMJ) cumulus parameterization scheme is employed only in the outer two domains (d01 & d02). A microphysical scheme namely the WRF single moment 6 class (wsm6) (*Hong and Lim*, 2006) is used for all the observed case simulations for reasons to be discussed in section 5. The model output from the observed case simulation is compared with the available observed meteorological parameters for validation. The daily rainfall information over the area considered for this study is obtained from TRMM-3B42 datasets and surface measurements from the Indian Meteorological Department (IMD).

As the main objective of this paper is to evaluate the microphysical processes and their possible dynamical feedback in electrically distinguished rainfall events, the accurate electrical characterizations of the events is important. The electrical distinguishability of clouds can be ascertained in two ways: either through measurement of the surface electric field below the storm or by ensuring the presence/absence of lightning near the observatories. The presence of lightning in the vicinity of the observatory ensures a stronger electrical environment inside the cloud. For the rain events observed at the HACPL, the electrical distinguishability of the events is ascertained by observing the lightning activity near the HACPL with the Maharashtra

Lightning Location Network (MLLN) as there is no measurement of the surface electric field available at the observatory. The measurement of the surface electric field during storms observed at the AEO was carried out with an electric field mill. The field mill was kept in a pit with its sensor flush with the ground. Interested readers are referred to *Mudiar et al*. (2021a) for the detailed measuring techniques of lightning and electric field. For the SE storms which are considered for simulation, some of the available cloud properties and meteorological features derived from the surface-based JW disdrometer and the Moderate Resolution Imaging Spectroradiometer (MODIS) (Terra platform) collection 6 (Baum et al., 2012) are documented in Table 1 along with the observed lightning flash rates from the MLLN.

3. **Results**

As extensive evidence regarding the electrical modification of raindrop size has already been reported in Mudiar et al. (2018, 2021a, 2021b, 2022), so here we will only focus on the implication of the presence of larger raindrops in the SE cloud. First, we will select two electrically distinguished rain events (one SE and one WE) and characterize them microphysically. Figure 2a and 2b depict the Height Time Index (HTI) of the radar reflectivity factor, Z for two rainfall events observed over the HACPL on 13 May 2015 and 4 October 2014, derived from the MRR. Both the events exhibit the initial convective and subsequent stratiform rainfall regimes. The stratiform regime is characterized by a prominent radar bright band at a MSL height of 4.3 km. The event shown in Figure 2a is characterized by the presence of lightning activity near the HACPL (see Figure 3), while for event 2b, no lightning activity was recorded by the MLLN in the neighborhood of the HACPL. Hence the event shown in Figure 2a is considered SE category and the event in Figure 2b is WE category. The lightning-producing storms observed in the pre- and post-monsoon season over the Indian subcontinent include air mass thunderstorms and squall lines. The time evolution of lightning on 13 May 2015 in the vicinity of the HACPL suggests that this SE storm is an air mass thunderstorm and is stationary in nature (see Figure S1 in supporting information). The corresponding rain rates are shown in Figure 2(c-d). While the convective regimes are characterized by heavy rain rate (>10 mm hr^{-1}), the stratiform regimes exhibit a lower rain rate (<10 mm hr^{-1}) consistent with the observation of Tokay and Short, (1996). The transition regime from convective to stratiform which is characterized by lower rainfall rate is evident in both events. The time evolution of the Mass-

weighted Diameter (MWD) of raindrops measured by the JWD depicted in Figure 2(e-f) shows the presence of significantly larger raindrops in the SE event compared to the WE event. This is consistent with many polarimetric radar observations of lightning-producing storms (Kumjian and Ryzhkov, 2008; Mattos et al., 2016). This is expected as explained above. The most contrasting feature between the SE and WE events can be seen in the time evolution of the rain intercept parameter (N_0) as shown in Figure 2(g-h). While the WE event exhibits a high frequency fluctuation in the time evolution of N_0, the SE event shows a relatively stable evolution of N_0 with a lower magnitude as well. The observed larger value of N_0 in the transition regime in both events is found to be consistent with Zhang et al., (2017). This distinction in N_0 is further explored in the section below from the microphysical perspective.

3.3 The characteristics of the rain intercept parameter N_0 in SE events

The values of N_0 depend primarily on the rain type and intensity (*Zhang et al*, 2008). A study over the HACPL by *Konwar et al*. (2014) also revealed that vertical variations of N_0 are distinct for the convective and stratiform regimes of clouds. It has been commonly observed that the value of N_0 increases with the rain liquid water content, W (*Zhang et al*, 2008, *Morrison et al*., 2012). At higher W, a larger number of raindrops formed by collision-coalescence of droplets produce a higher rain number concentration, thereby increasing the value of N_0. Figure 4(a) shows the scatter plot representation of N_0 as a function of W for 33 SE events observed over the HACPL. These two parameters are calculated from the corresponding RDSD measured by the disdrometer located at the HACPL following the method of moments as in Konwar et al. (2014). From this Figure, it can be seen that N_0 exhibits a decreasing trend with increasing values of W, albeit large scatter across W. It may be noted that because of the large variability in N_0, the trend looks weaker. A separate trend analysis between $\log(N_0)$ and W for the SE event reported in Figure 2a depicts a correlation coefficient, r=-0.64 indicating a significant trend between the two variables. See also Figure S2 in the supporting information A. This is in contrast to the observations of Zhang et al. (2008) and Morrison et al. (2012), but consistent with the observation of *Tokay and Short* (1996) who observed that the value of N_0 exhibits a decreasing trend with rainfall rate. The two events reported in Figure 2 have been superimposed in Figure 4(a). The similar characteristics of the event shown in Figure 4a (red dots), imply that this event can be treated as a representative sample of SE events. On the other hand, the event shown in the

right panel of Figure 2b (black square), exhibits the same characteristics as reported by *Zhang et al*. (2008) and *Morrison et al.* (2012).

The values of N_0 averaged over the entire rainy periods of all 33 SE events are shown in the bar graph representation in Figure 4(b). It can be seen that N_0 exhibits large variability among the events considered. This is consistent with the previous observation which shows that values of N_0 depend on the rain type and the intensity of convection (Zhang et al., 2017). For purposes of comparison, in the same Figure, we have overlaid the values of N_0 for 17 rain events for which no lightning was observed in a box of 100 km × 100 km. The absence of lightning indicates that these events may not be as strongly electrified as lightning-producing events. It can be seen that these WE events exhibit higher values of N_0 (mean= 68389 $m^{-3}mm^{-1}$) compared to the SE (N_0_mean=1649 $m^{-3}mm^{-1}$) events. This implies that SE rain events exhibit a lesser concentration of smaller raindrops than the WE counterpart. The SE electrified storms achieve this microphysical characteristic by virtue of enhanced collision-coalescence of raindrops below the melting layer. Numerous laboratory and numerical investigations have revealed that in the presence of an ambient electric field, raindrops collide more frequently relative to an electrically neutral condition by virtue of the electrical attraction (Schlamp et al.,1976; Pruppacher and Klett, 1996; Khain et al, 2004). It is also a known fact that two electrified colliding drops coalesce more easily than their neutral counterpart (Ochs and Czys 1987; Freier,1960). In the case of collision between electrified raindrops, the electrostatic attraction between the colliding raindrops enhances the drainage of the air film trapped between the drops which help the drops to coalesce permanently (Ochs and Czys, 1987). The efficient coalescence of smaller raindrops in the presence of an electric field resulted in a substantial reduction in the number concentration of smaller raindrops (Mudiar et al.,2021b) and hence the value of N_0.

As evident from the discussion above, two possible hypotheses can be considered to explain this distinct characteristic of N_0 in SE rain events, viz, the ice factory hypothesis and the electrically induced coalescence of raindrops below the melting layer. The melting of ice phase hydrometeors (for example graupel and hail), which invariably remain associated with SE clouds, will produce raindrops through three different processes

(1) Direct melting of graupel and hail.

This process results in large drops below the melting layer. While these large raindrops drift downward to the surface, they face collisional breakup, thereby producing numerous tiny raindrops in the warm phase of the storm along with the large raindrops (Friedrich et al. 2013; Raut et al., 2021). Also, during the convective regimes of a storm, a large amount of liquid water can be transported to the mixed-phase region of the storms by a stronger updraft, where ice crystals grow by the riming process. These rimed ice crystals result in an increase in the value of N_0 upon melting below the melting layer (Bringi et al., 2002).

(2) Shedding of raindrops from the surface of melting particles.

While melting, hail/graupel particles (diameter >19 mm) shed smaller drops in the diameter range from 0.5mm to 2.0 mm, with a modal diameter of 1 mm (Lesins et al., 1980, Rasmussen et al. 1984, Pruppacher and Klett, 1996, Ryzhkov et al., 2013). The shedding of drops from the surface of melting particles can produce 1000-2000 smaller drops (1mm) per kilometer below the melting layer (Pruppacher and Klett, 1996). This will result in an increase in the number concentration of smaller raindrops and hence in the value of N_0.

(3) Spontaneous break up of large raindrops.

This raindrop breakup process under the influence of aerodynamic forces will again result in numerous smaller raindrops (Low and List,1982a), thereby contributing positively to N_0.

Clear evidence of dominant raindrop breakup can be seen for the WE event in Figures 2f and 2h with a high-frequency fluctuation in the raindrop size and the values of N_0. On the other hand, electrically induced coalescence of drops below the melting layer systematically reduces the number of smaller raindrops, thereby effectively reducing the value of N_0 (see Figure 3f in Mudiar et al., 2021b). Evidently, we shall consider the electrically-induced coalescence of millimeter-sized raindrops as a dominant mechanism for reduction in the value of N_0 in the SE rain events relative to the WE ones, albeit the inherent uncertainty from the melting process. An important microphysical implication of this observation is that WE events will exhibit a larger rain evaporation rate than the SE events as explained in *Morrison et al*. (2009). This aspect has been explored further in the next section.

3.4 The effect of electrification on the rain evaporation rate

Rain evaporation is a major sink of the latent heat released by the condensation of water vapor. The available latent heat also transforms to kinetic energy of updraft. If the vapor density at the surface of cloud/raindrops exceeds the vapor density of the ambient environment, evaporation of the drops takes place as vapor is diffused away from the drops. It is known that smaller drops evaporate faster than larger drops because the rate of change of drop size through evaporation is inversely proportional to the drop radius (*Pruppacher and Klett*, 1996). As explained above, the SE cloud exhibits fewer smaller raindrops relative to the WE counterpart. One major anticipated implication of this distinct RDSD in both types of cloud may be the change in rain evaporation rate below the melting layer. A significant impact of the rain intercept parameter N_0 on the rain evaporation rate is well known (*Morrison et al*., 2009). The rate of evaporation may be calculated from the RDSD parameter using the following equation (*Reisner et al*., 1998)

$$\left(\frac{\partial q_r}{\partial t}\right)_{EVAP} = \frac{2\pi N_{0r}(S-1)}{A'+B'}\left\{\frac{0.78}{\lambda^2} + 0.31\left(\frac{a_r\rho}{\mu}\right)^{1/2}\frac{\Gamma(b_r/2+5/2)}{\lambda^{b_r/2+5/2}}\right\} \quad (1)$$

Here, q_r is the rain mixing ratio (kg kg^{-1}), N_{0r} (m^{-4}) is the RDSD intercept parameter, S is the saturation ratio of liquid water, A' and B' are the thermodynamic parameters associated with the release of latent heat, λ (m^{-1}) is the slope parameter of the RDSD, a_r and b_r are the parameters related to the fall speed of the rain (fall speed for a given diameter D can be expressed as $a_r D^{b_r}$), μ (kg m^{-3} s^{-1}) is the dynamic viscosity of air, ρ is the air density (kg m^{-3}) and Γ is the gamma function. This equation is similar to the ones appearing in *Rutledge and Hobbs* (1983) and *Morrison et al*. (2009).

Figure 5 depicts the rain evaporation rate (ER) below the melting layer calculated by using equation (1) for both the SE and WE events reported in Figure 2. The evaporation rate is calculated from the MRR-derived RDSD averaged over the entire stratiform regimes. Considering the large attenuation of the MRR signal in the heavy rainfall regimes (see *Konwar et al*., 2014, *Mudiar et al*., 2018), the convective parts of the events (R> 10 mm hr $^{-1}$) are avoided in the analysis of rain evaporation rate. This analysis with the MRR is limited to the domain below the MSL height of 4 km to avoid the presence of ice phase hydrometeors, as Figure 2 shows the

presence of the melting layer at 4.6 km MSL height. A significant reduction in the evaporation rate is observed below 3.6 km MSL height for the SE event. This is expected because the SE events depict the presence of more number of larger raindrops and a lesser concentration of smaller drops below the melting layer than the WE events, as shown in *Mudiar et al*. (2018). Although the convective regimes (R>10 mm hr^{-1}) are avoided for ER analysis considering a significant attenuation of MRR signal in larger rainfall rates (*Peters et al*., 2005), a qualitative analysis can be made. *Kessler* (1974) has parameterized the rain evaporation rate as $ER \propto N_0^{0.35}$. Since the convective regimes are known to produce a larger value of N_0 (Waldvogel, 1974, Tokay and Short,1996, Zhang et al., 2017) relative to the stratiform counterpart, it follows that the convective regimes will exhibit a larger magnitude of ER depending upon the ambient relative humidity (see equation 1). For the events reported in Figure 2, the respective mean values N_0 for the convective regimes of the SE and WE events are observed to be 4975 and 10718 in the units of m^{-3} mm^{-1}. Hence, a larger magnitude of rain evaporation rate may be expected for the WE event depending upon the ambient relative humidity.

Recent observation shows that surface-measured electric field and raindrop size remain positively correlated. The greater the electric field, the larger will be the raindrops (*Mudiar et al*., 2021b). As there were no electric field measurements for the events shown in Figure 2 at the HACPL, we could not analyze the effect of the electric field on the rain evaporation rate for those events. However, simultaneous measurements of surface electric field and RDSD were available for some of the storms observed over the AEO, in Pune. A few such storms were observed over the AEO on 3 June, 31 August, 8 Sept. and 9 Sept. 2008. While the electric field was measured with an electric field mill (*Pawar et al*., 2017), the RDSD was measured with an optical disdrometer. The magnitude of surface measured electric field for the events considered varies from 0-5000 V m^{-1} with an observed peak lightning rate of 22 flashes per minute during the mature stage of one of the storms (the storm in Figure 6a). The electric field traces for these storms are shown in Figure S3 in the supporting information along with the peak lightning rates. Figure 6(a-d) depicts the bar graph representation of the N_0 values as a function of the electric field. The time resolution of the disdrometer measurement was 10 seconds. The measured values of N_0 are grouped in bins of electric field of width 500 V m^{-1} for all events. The bars on the graphs represent the mean values of the bins. As expected, at larger magnitudes of E field, N_0 exhibits lower values for each of the storms considered. This indicates that at a larger magnitude

of electric field, the number of smaller raindrops is reduced substantially in the RDSD spectrum. This can be attributed to the increased coalescence of the smaller drops to form bigger ones as explained in *Mudiar et al*. (2021b). It is may be noted here that the event in Figure 6a exhibited a much larger lightning rate (22 fl. min^{-1}) compared to the rest of the events (3 fl. min^{-1}) and hence a more vigorous ice factory. Also, this event exhibited a lower value of N_0 relative to the rest of the events. For this storm, N_0 exhibits an increasing trend with the lightning rate (see Figure S4 in the supporting information) which is expected considering a more vigorous ice factory at a larger lightning rate. The plausible reason for the smaller value of N_0 for this storm relative to the rest of the storms may be a much larger magnitude of the E field (Emax= 5000 Vm^{-1}) relative to the other events shown in Figure 6b-d (Emax= 1800 Vm^{-1}).

A reduction in smaller raindrop numbers strongly indicates a reduction in the rain evaporation rate as well. The corresponding bar plot of rain evaporation rate as a function of E field (Figure 6e-h) clearly indicates that rain evaporation rate (ER) decreases at the larger magnitude of the electric field. The reduction of rain evaporation rate at a larger magnitude of electric field can be attributed to two physical processes

(a) The electrically enhanced coalescence of raindrops substantially reduces the number concentration of smaller raindrops below the melting layer. The larger the magnitude of the electric field, the lesser the number concentration of smaller drops (resulting in smaller value of N_0) as can be seen from Figure 6. This results in a reduction in ER as smaller drops tend to evaporate faster.

(b) It has been shown that the electrical attraction between the charged raindrops and the molecular dipoles of water vapor oriented along the electric field (produced by the charged raindrops) may create a water concentration gradient close to the raindrops (*Nielsen et al*, 2011). This charge-dipole interaction may result in a reduction in ambient saturation vapor pressure over electrified raindrops thereby protecting the drops from evaporation. However, a quantitative estimation of this process for millimeter-sized raindrops has yet to be achieved.

The analysis presented in this section clearly indicates that the raindrop evaporation rate is significantly lowered by the electrification of cloud. This microphysical modification might have important consequences for the cloud dynamics and rain formation. A net evaporation depletes the rain water content, thereby affecting the quantitative precipitation estimation (QPE) (*Kumjian and Ryzhkov*, 2010). A WRF simulation study by *Morrison et al*. (2009) shows that reduced rain evaporation enhances the rainfall amount in the trailing stratiform region of an idealized squall line. They also mentioned that the reduced evaporation rate leads to a reduction in latent cooling in the convective regime, thereby increasing the mean convective updraft intensity. The negative buoyancy produced by evaporative cooling can influence the storm evolution by producing enhanced downdraft (*Srivastava*, 1985, 1987).

As the reduction in the values of N_0 in SE events reduces the rain evaporation rate, it is important to investigate the possible feedback it can give to the cloud processes. The cloud-resolving models (CRM) are widely used tools to study cloud processes. To evaluate the microphysical and dynamical implications of a reduced N_0 and consequent evaporation rate in the SE rain events, we have performed some numerical experiments using the WRF model. Two sets of experiments are performed: an idealized 2D simulation and two 3D observed case simulations. The chosen observed SE events for the simulation study are the one shown in Figure 2a (13 May 2015) and another one observed at the HACPL on 5 May 2015. The results of the numerical simulation will be presented next.

3.5 Results from Numerical Simulation Experiments

A. Idealized simulation

As mentioned in section 2, for the numerical experiment, we have used the WRF model which has been extensively used to study cloud processes. *Morrison et al*. (2009) investigated the effect of the rain evaporation rate on the microphysics and dynamics of an idealized storm with WRF 2D squall-line simulations. In the WRF model, the cloud and precipitation size distribution are represented by a gamma distribution

$$N(D) = N_0 D^{\mu} e^{-\lambda D} \qquad (2)$$

Where N_0 , λ, μ represents the intercept, slope and shape parameters of the RDSD, respectively. D indicates the diameter of the particles.

Considering μ=0 for rain following *Morrison et al.* (2008), the size distribution of rain can be expressed as an exponential function

$$N(D) = N_0 e^{-\lambda D} \quad (3)$$

This is commonly known as Marshall-Palmer distribution of raindrops.

The one moments (1M) scheme implemented in the WRF model predicts the mass mixing ratio (q) of five hydrometeor species, including cloud droplets, cloud ice, snow, rain, and graupel. A value of N_0 is specified in the physics scheme. The number of hydrometors species, N and λ can be derived from the predicted q and specified N_0 using equations (4) and (5).

$$\lambda = \left(\frac{\pi \rho_r N}{q\rho}\right)^{1/4} \quad (4)$$

$$N_0 = N \lambda \quad (5)$$

Where ρ_r is the density of raindrops (1000 kg m^{-3}) and ρ is the air density (kg m^{-3}).

As the purpose of this study is to evaluate model sensitivity to electrically modified N_0, we have decided to use the one moment scheme where we can specify the value of the observed N_0 in the model physics. For our study, we use the WRF single moment six class scheme (wsm6) as explained in *Hong and Lim* (2006). In this scheme, the default value of N_0 is specified as $8 \times 10^6\ m^{-4}$. This value is widely used for the representation of warm rain (Kessler, 1969).

Following *Morrison et al*. (2009), we choose a single 2D domain for the idealized simulation. The grid in both x and y directions is 99 points with a grid spacing of 11m. The model has been initialized using the default input-sounding provided with the WRF for 2D squall line simulations. All the physics options are turned off except for the microphysics (from wsm6). As the initialization is performed with an idealized input sounding, the simulated outputs are not compared with the observations. This experiment serves to produce a simplified interpretation of the results in the absence of the other physics scheme such as radiation physics, cumulus physics and planetary boundary layer physics. Two experiments are carried out: one with the default

value of N_0 ($= 8 \times 10^6\, m^{-4}$), the other one with a new value of N_0 ($= 1.6 \times 10^6\, m^{-4}$). This value is the mean of all the SE events shown in Figure 4(b). The statistics of N_0 for these SE events are depicted in a box plot representation in Figure S5 in the supporting materials.

As explained by *Morrison et al*. (2009), a reduction in the value of N_0 should enhance the rain rate at the surface. In Figure 7(a), we have compared the accumulated rain from the two experiments. The default scheme is designated 'wsm6', while the modified run (with N_0 $= 1.6 \times 10^6\, m^{-4}$) is designated 'wsm6(M)'. As can be seen, 'wsm6(M)' produces a substantially larger amount of rain compared to 'wsm6', although the rain is delayed by 3 hours in wsm6(M). The factor which can potentially enhance the rain rate is the reduced rain evaporation as explained by *Morrison et al.* (2009). As expected, the wsm6(M) exhibits a reduced rain evaporation rate relative to the wsm6 as can be seen from Figure 7(b). But can this much reduction in evaporation rate increase the rain amount so high or are other mechanisms also contributing? What are the consequences of this reduced evaporation rate on storm dynamics?

Morrison et al. (2009) stated that the evaporation rate can influence the intensity of the convective updraft. They explained that a lower value of N_0 produces a lower evaporation rate which leads to the reduction in latent cooling, thereby increasing the mean convective updraft intensity. Rain evaporation is a major sink of the latent heat released by condensation and vapor deposition. *Tao and Li* (2016) suggested that the more the rain, the stronger will be latent heat release or we can argue conversely: the stronger the latent heat release, the greater the rainfall. An enhanced latent heat release can induce a stronger updraft. To investigate the effect of reduced N_0 in wsm6(M), we have plotted the simulated maximum vertical velocity (W_{max}) in Figure 7(c). It has been observed that wsm6(M) produces substantially larger updraft velocity relative to wsm6, especially in the middle and upper troposphere. One possible cause of this may be the release of more latent heat (indicated by higher rain amount) to induce stronger convective intensity. However, it is important to consider the fact that a change in buoyancy by latent heating may get balanced approximately by condensate loading (see *Grabowski and Morrison*, 2020). The other possible cause is the reduction in rain evaporation rate, a consequence of lower N_0 (Snook and Xue, 2008; *Morrison et al*., 2009). This may happen primarily below the melting layers of the SE cloud. An updraft intensity of such magnitude (10-25 m s^{-1}) is typical of lightning-producing clouds (*Williams*, 2001). It has also been observed that while wsm6

497 produces maximum vertical velocity in the 2nd hour of model integration, wsm6(M) produces
498 maximum vertical velocity in the 4th hour of model integration. This indicates a feedback to
499 cloud vertical velocity from the microphysics in wsm6(M). The idealized simulation experiment
500 shows that a change in the value of N_0 may have important implications for simulated rain
501 accumulation and updraft intensity.

502

503 **B. Simulation of observed SE event**

504 As the idealized simulation experiment incorporating values of N_0, characteristic of SE
505 events shows a larger rain amount, we are curious to see the effect of N_0 modification in an
506 observed SE event. For that, we have chosen the same SE event shown in Figure 2(a) for the
507 simulation. Some of the meteorological and electrical features for this storm have been
508 documented in Table 1. This storm exhibited a maximum rain rate of 22 mm hr^{-1} with a lightning
509 rate of 4 flashes min^{-1}. Two experiments have been performed: one with the default value of N_0
510 ($= 8 \times 10^6\, m^{-4}$), and the other one with a new value of N_0 ($= 1.6 \times 10^6\, m^{-4}$) obtained from
511 observations of SE storms. Figure 8(a) depicts the rain rates from both the simulations averaged
512 over a 25km×25km box centered at the HACPL. As before, the default scheme is indicated as
513 'wsm6', while the modified run is designated as 'wsm6(M)'. A significantly larger rain rate is
514 observed in wsm6(M) relative to wsm6. This selection of the 25km×25km box is made based on
515 the fact that a larger domain may contain different cloud systems: some are SE and some are
516 WE. As we have perturbed the model physics with a value of N_0 averaged over only the SE
517 events, the inclusion of any probable WE events in the process of spatial averaging may bring
518 inconsistency to the interpretation of the simulated fields. For a comparison, the JWD measured
519 rain intensity at the HACPL is overlaid along with the simulated rain intensities. It may be noted
520 here that, the maximum rain rate observed at the HACPL, may not be a correct representation of
521 the maximum rain rate observed during the storm. A better comparison of accumulated rain rate
522 from observation and simulations has been depicted in Figure 8(b). In this Figure, the
523 accumulated rain averaged over the box from both the simulation experiments have been
524 compared with the observed rain aacumulation obtained from Indian Meteorological Department
525 (IMD) and Tropical Rain Measuring Mission (TRMM) 3B-42 precipitation datasets. Some
526 improvement in the accumulated rain is also observed with wsm6(M). The idealized simulation

suggests that this improvement may be due to the reduced rain evaporation rate in wsm6(M). This increase in rain rate by virtue of reduced rate of rain evaporation is found to be consistent with the modeling study of *Tao and Li* (2016). A persisting problem in simulating the observed frequency distribution of tropical rainfall by most of the weather/climate models is that the models tend to highly overestimate the frequency of very light rain, and substantially underestimate the frequency of heavy rainfall events (*Goswami and Goswami,* 2016). This study indicates that a proper prediction of the rain intercept parameter, N_0 in models may improve the frequency distribution of heavier precipitation.

The results from the idealized simulations as well as the observed case simulations presented above show that an appropriate modification of the rain intercept parameter N_0 (characteristics of SE) can enhance the intensity and the amount of simulated rainfall. The primary cause of this can be attributed to the reduction in rain evaporation rate introduced in the model by the applied modification. However, as mentioned before, a reduction in rain evaporation rate will also increase the net latent heating in the warm phase of the cloud. This may give positive feedback to the cloud updraft by delaying the evaporative-driven downdraft. This argument is consistent with the profile of maximum vertical velocity obtained from the idealized simulation where it is shown that wsm6(M) produces significantly higher vertical velocity in the mid and upper troposphere. From the observed case simulation, we have tried to investigate the storm temporal evolution from a height time index (HTI) plot of area-averaged (25km×25m box) vertical velocity produced by wsm6 and wsm6(M) as shown in Figure 9(a-b). At the beginning of the storm (cumulus stage, 11.30-13.30 IST), larger vertical velocity can be seen in the lower troposphere from both simulations as expected. A common observation of the SE storm suggests the presence of a stronger updraft (9-10 ms^{-1}) in the cumulus phase (*Roger and Yau*, 1989). At 15.30 IST, both simulations show the presence of the strongest updraft from 4.5 km to 9.5 km. The presence of the 0^o C level at 4.5 km indicates that this region of strongest updraft is in the mixed-phase region of the cloud. The presence of a stronger updraft in the mixed-phase cloud is considered essential for charge separation through the non-inductive charging mechanism (*Takahashi*, 1978). However, the contrasting difference between the two simulations is the expanded updraft core in wsm6(M) in the mixed-phase region. This can be explained by considering the reduced rain evaporation rate (*Morrison et al*., 2009). This reduction increases the updraft intensity in wsm6(M), as evident from Figure 9(b) relative to 9(a). Please note that

while wsm6 produces downdraft at the lower altitudes from the 2nd hour of the simulated storm (13:30 IST), wsm6(M) delays the onset of downdraft to the 5th hour (16:30 IST). This is a direct consequence of reduced latent cooling in wsm6(M). At the later stage of the storm, a weaker updraft prevails in the upper troposphere (Figure 9), while the stronger downdraft can be observed at the lower level, possibly induced by the melting of ice phase hydrometeors (*Houze*, 1997). To establish the robustness of the proposed hypothesis, we have carried out a simulation of another SE event (5 May 2015) observed over the HACPL with the same model set up. The accumulated rain (averaged over the 25km×25m box) for both the observed case simulations are documented in Table 1. The modified simulation shows a 76% increase in rain accumulation. Figure 10(a-b) depicts the HTI plot of area-averaged (25km×25m box) vertical velocity produced by wsm6 and wsm6(M), respectively. This Figure also shows that simulation with 'wsm6(M)' delays the initiation of downdraft relative to the simulation with 'wsm6', consistent with the hypothesis of updraft enhancement by reduced rain evaporation rate as in Figure 9(a-b). These findings are consistent with the results from an idealized squall line simulation of *Morrison et al*., (2009). The domain averaged mass mixing ratio of ice phase hydrometeors (ice+graupel+snow) exhibits approximately 26% increase with wsm6(M) relative to wsm6, consistent with the increased updraft intensity (see Table 1). The results from these simulation studies add confidence to our conclusion that a reduction in rain evaporation rate in SE rain events (a consequence of the electrically modified value of N_0) suppresses/delays the downdraft, thereby invigorating the convection.

4. Discussions

Precipitation and cloud electrification, while both are the product of convective instability in the atmosphere, both exhibit different sensitivity to the convective intensity (*Williams*, 2005). However, both can feedback on each other through different microphysical and dynamical processes. The role of precipitation on cloud electrification has been extensively discussed by *Williams and Lhermitte* (1983). They suggest that falling precipitation could substantially contribute to storm electrification. However, the effect of cloud electrification on precipitation microphysics has only been addressed recently. In a series of paper, *Mudiar et al*. (2018, 2021a, 2021b) have shown that the cloud electric field could indeed substantially enhance the growth of raindrops. As shown here, because of the electrical enlargement of raindrops, the rain intercept

parameter N_0 is reduced considerably in clouds that are associated with a stronger in-cloud electric field, such as lightning-producing clouds. The reduction of N_0 consequently reduces the rain evaporation rate, thereby further enhancing the convective intensity of storms. An analytical discussion of storm invigoration as a consequence of reduced rain evaporation rate has been presented below.

Conditional instability, the thermodynamic basis for thunderstorm formation, is driven primarily by Convective Available Potential Energy (CAPE). However, the generation of thunderstorms may also occur in low CAPE conditions depending upon orography and prevailing meteorological conditions (*Murugavel et al*., 2014). The CAPE can be defined as the accumulated buoyant energy from the level of free convection (LFC) to the equilibrium level (EL) (*Williams and Renno*, 1993)

$$CAPE = \int_{LFC}^{EL} R_d\left(T_{vp} - T_{ve}\right) d\ lnp \qquad (6)$$

The parcel and environmental virtual temperature are T_{vp} and T_{ve} respectively, R_d is the gas constant of dry air and p is the pressure. A reasonable correlation between CAPE and the total number of lightning flashes is well recognized (*Pawar et al*., 2012), as the interplay among CAPE, vertical updraft and cloud microphysics dominantly influence the cloud electrical activity and lightning (*Williams*, 2001). Larger CAPE values produce conditional instability in the atmosphere, thereby facilitating vigorous convection with active mixed-phase microphysics and larger lightning activity (*Williams et al*., 1992). *Emanuel et al.* (1994) suggest that the virtual temperature remains associated with the boundary-layer entropy. They also suggest that the convective downdraft acts to reduce the boundary-layer entropy. The reduced rain evaporation rate in wsm6(M) will essentially reduce the latent cooling and thereby delays the downdraft at the lower level at the earlier stage of the storm, as evident from Figures 9(b) and 10(b). An inhibition in a convective downdraft in wsm6(M) will essentially result in larger boundary-layer entropy. *Williams and Renno* (1993) reported that boundary layer entropy and CAPE remain well correlated in the tropical atmosphere.

Also, when the precipitation particles fall to the sub cloud layer, the evaporation contributes to the negative thermal buoyancy. As wsm6(M) is associated with a lower value of N_0 than wsm6, hence the previous scheme should produce a lower evaporation rate as the storm

evolves. The lower rain evaporation rate delays the downdraft by reducing the latent cooling, thereby increasing the convective intensity (see *Morrison et al*., 2009). As this storm invigoration comes from a reduced rain evaporation rate, a consequence of electrical enhancement of raindrops size accompanied by a reduction in the number of smaller drops, we are encouraged to term this positive feedback between microphysics and dynamics of the storm as '*Dynamical Invigoration of Electrified Storms*'. The proposed hypothesis has been schematically represented in Figure 11. A potential implication of these results can be discussed from the perspective of tornadogenesis. It has been reported that RDSD with larger raindrops (smaller N_0) favors tornadogenesis by weakening the cold pool through reduced evaporation (*Snook and Xue*, 2008). It is known that the initiation of a tornado in a supercell storm is preceded by vigorous lightning (*MacGorman and Burgess*, 1994). The electrification of the storm may act to reduce the rain evaporation rate, thereby assisting in tornadogenesis. However, this needs further investigation as no convincing observational evidence of this process has been reported yet.

5. Conclusion

The investigation of the hypothesis for the influence of cloud electrification on the dynamics of tropical clouds using observational datasets and numerical experiments has resulted in the following conclusions:

1. Initiated by convective instability, SE clouds with high lightning propensity are associated with larger concentration of bigger raindrop and lesser concentration of smaller raindrop and hence a reduced value of the RDSD intercepts parameter N_0 relative to the WE clouds.
2. The depletion of N_0 results in a reduction of rain evaporation rate in clouds associated with a stronger electrical environment.
3. The reduction in rain evaporation rate suppresses/delays the downdraft, thereby further invigorating the convection.
4. The findings here strongly suggest that the representation of the lightning-producing and non-lightning-producing clouds in weather/climate models should be distinct.

Acknowledgments:

IITM is funded by the Ministry of Earth Sciences, Government of India. We thank the Director, IITM for his support and encouragement. BNG thanks the Science and Engineering Board (SERB), Government of India, for the SERB Distinguished Fellowship and a research grant. We sincerely thank the scientific and support staff working at the HACPL. The authors thank the following data sources for making the data available: NCEP global final analysis data (http://dss.ucar.edu/datasets/ds083.2/), TRMM data products from STORM-PPS (https://storm.pps.eosdis.nasa.gov/storm/), and Indian met department gridded rainfall products.

Open Research

The observational data used to prepare the manuscript can be found in the link https://osf.io/MWCAV/.

References:

Baum, B. A., W. P. Menzel, R. A. Frey, D. Tobin, R. E. Holz, S. A. Ackerman, A. K. Heidinger, and P. Yang (2012) MODIS cloud top property refinements for Collection 6, J. Appl. Meteorol. Climatol., 51, 1145–1163.

Bhalwankar, R.V., Sathe, A.B. and Kamra, A.K (2004). The evaporation of the charged and uncharged water drops suspended in a wind tunnel. *J Earth Syst. Sci*. **113,** 129–138 https://doi.org/10.1007/BF02709783.

Boers N, Bookhagen B, Barbosa H, Marwan N, Kurths J and Marengo J (2014). Prediction of extreme floods in the Eastern Central Andes based on a complex networks approach. *Nat Commun* 5:5199. doi: 10.1038/ncomms6199

Bringi, V. N., Chandrasekar, V., Hubbert, J., Gorgucci, E., Randeu, W. L., & Schoenhuber, M. (2003). Raindrop Size Distribution in Different Climatic Regimes from Disdrometer and Dual-Polarized Radar Analysis, *Journal of the Atmospheric Sciences*, *60*(2), 354-365

Bruning, E.C., Rust, W.D., Schuur, T.J., MacGorman, D.R., Krehbiel, P.R. and Rison, W., (2007). Electrical and polarimetric radar observations of a multicell storm in TELEX. *Mon. Weather Rev*. 135, 2525–2544. http://dx.doi.org/10.1175/MWR3421.1.

Bruning, E.C., Rust, W.D., MacGorman, D.R., Biggerstaff, M.I. and Schuur, T.J.(2010). Formation of charge structures in a supercell. *Mon. Weather Rev*. 138, 3740–3761.

Carey, L. and S. Rutledge(2000). "The Relationship between Precipitation and Lightning in Tropical Island Convection: A C-Band Polarimetric Radar Study." *Monthly Weather Review* 128 : 2687-2710.

Choudhury B.A., B.N. Goswami, Yasmin Zahan, P.V. Rajesh,(2021). Seasonality in power law scaling of convective and stratiform rainfall with lightning intensity over Indian Monsoon regions, *Atmospheric Research,* 248,105265, ISSN 0169-8095.

Christian H., C. R. Holmes, J. W. Bullock, W. Gaskell, A. J. Illingworth, and J. Latham (1980). Airborne and ground-based studies of thunderstorms in the vicinity of Langmuir Laboratory, *Q. J. R. Meteorol. Soc*., 106, 159-174.

Dee, D. P., Uppala, S. M., Simmons, A. J., Berrisford, P., Poli, P., Kobayashi, S., et al. (2011) The ERA-interim reanalysis: Configuration and performance of the data assimilation system. Quarterly Journal of the Royal Meteorological Society, 137(656), 553–597. https://doi.org/10.1002/qj.828

Dudhia, J. (1989). Numerical study of convection observed during the winter monsoon experiment using a mesoscale two dimensional model. *J. Atmos. Sci*., 46, 3077–3107.

Emanuel, K.A., David Neelin, J. and Bretherton, C.S. (1994). On large-scale circulations in convecting atmospheres. *Q.J.R. Meteorol. Soc*., 120: 1111-1143. https://doi.org/10.1002/qj.49712051902

Friedrich, K., Kalina, E. A., Masters, F. J., & Lopez, C. R. (2013). Drop-Size Distributions in Thunderstorms Measured by Optical Disdrometers during VORTEX2, *Monthly Weather Review, 141*(4), 1182-1203

Freier, G. (1960), The coalescence of water drops in an electric field, *J. Geophys. Res.*, 65, 3979-3985.

Giannaros, T. M., Kotroni, V., and Lagouvardos, K. (2015). Predicting lightning activity in Greece with the Weather Research and Forecasting (WRF) model. *Atmospheric Research*, 156, 1–13.

Goswami B.B., B.N.(Goswami 2016). A Road Map for Improving Dry-Bias in Simulating the South Asian Monsoon Precipitation by Climate Models, *Climate Dynamics*, DOI:10.1007/s00382-016-3439-2

Grabowski, W. W. (2015). Untangling microphysical impacts on deep convection applying a novel modeling methodology, *J. Atmos. Sci.*, **72**, 2446– 2464.

Grabowski, W. W., & Morrison, H. (2020). Do Ultrafine Cloud Condensation Nuclei Invigorate Deep Convection?, *J. Atmos Sci*, *77*(7), 2567-2583.

Hazra, A., B. N. Goswami, and J.-P. Chen (2013). Role of interactions between aerosol radiative effect, dynamics, and cloud microphysics on transitions of monsoon intraseasonal oscillations, *J. Atmos. Sci*., 70, 2073–2087, doi:10.1175/JAS-D-12-0179.1.

Hong, S.-Y., and J.-O. J. Lim (2006). The WRF single-moment 6-class microphysics scheme (WSM6), *J. Korean Meteor. Soc*., 42, 2, 129–151.

Houze, R. A. (1997). Stratiform precipitation in regions of convection: A meteorological paradox? *Bull. Am. Meteorol. Soc*., 78(10), 2179–2196.

Joss, J. & Waldvogel, A. PAGEOPH (1967). 68: 240. doi: 10.1007/BF00874898

728 Khain, A., M. Arkhipov, M. Pinsky, Y. Feldm an, and Y. Ryabov (2004). Rain enhancement and
729 fog elimination by seeding with charged droplets. Part 1: Theory and numerical simulations,
730 J. Appl. Meteorol., 43, 1513–1529, doi:10.1175/JAM2131.1.
731
732 Konwar, M., S. K. Das, S. M. Deshpande, K. Chakravarty, and B. N. Goswami (2014).
733 Microphysics of clouds and rain over the Western Ghat, J. Geophys. Res. Atmos., 119, doi:
734 10.1002/2014JD021606.
735 Kumjian, M. R., and A. V. Ryzhkov (2010). The impact of evaporation on polarimetric
736 characteristics of rain: Theoretical model and practical implications. *J. Appl. Meteor.*
737 *Climatol.*, 49, 1247–1267.
738 Kumjian, M. R., & Ryzhkov, A. V. (2008). Polarimetric Signatures in Supercell
739 Thunderstorms, *Journal of Applied Meteorology and Climatology*, *47*(7), 1940-1961
740
741 Kessler, E (1969). On the Distribution and Continuity of Water Substance in Atmospheric
742 Circulations. *Meteor. Monogr*., No.32, *Amer. Meteor. Soc*.,84 pp.
743
744 Kessler, E., (1974). Model of precipitation and vertical air currents. *Tellus,* **26,** 519–542.
745
746 Khain, A., Rosenfeld, D., and Pokrovsky, A (2005). Aerosol impact on the dynamics and
747 microphysics of deep convective clouds. *Quarterly Journal of the Royal Meteorological*
748 *Society*, 131(611):2639–2663, ISSN 00359009. doi: 10.1256/qj.04.62.
749
750 Kumar, V. V., C. Jakob, A. Protat, C. R. Williams, and P. T. May (2015). Mass-flux
751 characteristics of tropical cumulus clouds from wind profiler observations at Darwin,
752 Australia, *J. Atmos. Sci.*, **72**, 1837– 1855, doi:10.1175/JAS-D-14-0259.1
753

754 Lesins, G. B., , R. List, , and P. I. Joe, (1980). Ice accretions. Part I: Testing of new atmospheric
755 icing concepts. *J. Rech. Atmos.*, **14**, 347–356.
756
757 Lhermitte, R. M., and E. R. Williams (1985). Thunderstorm electrification: A case study, *J.*
758 *Geophys. Res.*, 90, 6071-6078.
759
760 Liu, C., E. R. Williams, E. J. Zipser, and G. Burns (2010). Diurnal variations of global
761 thunderstorms and electrified shower clouds and their contribution to the global electrical
762 circuit, *J. Atmos. Sci*.,67, 309–323,doi:10.1175/2009JAS3248.1.
763
764 Löffler-Mang, M., and J. Joss (2000). An optical disdrometer for measuring size and velocity of
765 hydrometeors, *J. Atmos. Oceanic Technol*., 17, 130–139.
766 Low, T. B., and R. List, (1982a) Collision, coalescence, and breakup of raindrops. Part I:
767 Experimentally established coalescence efficiencies and fragment size distributions in
768 breakup. J. Atmos. Sci., 39, 1591–1606, doi:10.1175/ 1520-
769 0469(1982)039,1591:CCABOR.2.0.CO;2.
770
771 MacGorman, D. R., & Burgess, D. W. (1994). Positive Cloud-to-Ground Lightning in Tornadic
772 Storms and Hailstorms, *Monthly Weather Review*, *122*(8), 1671-1697
773
774 Mattos, E. V., L. A. T. Machado, E. R.Williams, and R. I. Albrecht (2016). Polarimetric radar
775 characteristics of storms with and without lightning activity, *J. Geophys. Res. Atmos*.,
776 121,14,201–14,220, doi:10.1002/ 2016JD025
777
778 Markowski, P. M., , J. M. Straka, , and E. N. Rasmussen (2003). Tornadogenesis resulting from
779 the transport of circulation by a downdraft: Idealized numerical simulations. *J. Atmos.*
780 *Sci.*, **60 ,** 795–823.
781
782 Mlawer, E.J., Taubman, S.J., Brown, P.D., Iacono,M.J., Clough, S.A. (1997) Radiative transfer
783 for inhomogeneous atmosphere: RRTM, a validated correlated-kmodel for the long-wave. J.
784 *Geophys. Res.* 102, 16663–16682. http://dx.doi. org/10.1029/97JD00237.

Morrison, H., G. Thompson, and V. Tatarskii (2009). Impact of cloud microphysics on the development of trailing stratiform precipitation in a simulated squall line: Comparison of one- and two-moment schemes. *Mon. Wea. Rev.*, **137,** 991–1007

Morrison, H., Tessendorf, S. A., Ikeda, K., and Thompson, G. (2012). Sensitivity of a simulated midlatitude squall line to parameterization of raindrop breakup. *Monthly Weather Review*, 140, 2437–2460.

Mudiar, D., Pawar, S. D., Hazra, A., Konwar, M., Gopalakrishnan, V., Srivastava, M. K., and Goswami, B. N. (2018). Quantification of observed electrical effect on the raindrop size distribution in tropical clouds. *Journal of Geophysical Research: Atmospheres*, 123. https://doi.org/10.1029/2017JD028205

Mudiar D., S.D. Pawar, A Hazra, V. Gopalkrishnan, D.M. Lal, K. Chakravarty, M. A. Domkawale, M. K. Srivastava, B.N. Goswami, and E. Williams (2021a), Lightning and precipitation: The possible electrical modification of observed raindrop size distributions, *Atmospheric Research*, Volume 259, 2021, 105663, ISSN 0169-8095, https://doi.org/10.1016/j.atmosres.2021.105663.

Mudiar, D., Hazra, A., Pawar, S. D., Karumuri, R. K., Konwar, M., Mukherjee, S., et al. (2022). Role of electrical effects in intensifying rainfall rates in the tropics. *Geophysical Research Letters*, 49, e2021GL096276. https://doi. org/10.1029/2021GL096276

Murugavel, P., Pawar, S.D. and Gopalakrishan, V. (2014), Climatology of lightning over Indian region and its relationship with convective available potential energy. Int. J. Climatol., 34: 3179-3187. https://doi.org/10.1002/joc.3901

Mudiar, D., Pawar, S. D., Gopalakrishnana, V., and Williams, E. (2021b). Electric Field Enlarges Raindrops beneath Electrified Clouds: Observational Evidence. *Geophysical Research Letters*, 48, e2021GL093577. https://doi.org/10.1029/2021GL093577

Nielsen J.K., C. Maus, D. Rzesanke and T. Leisner (2011). Charge-induced stability of water droplets in subsaturated environment, *Atmos. Chem. Phys*., vol. 11, no. 5, 2031–2037.

Ochs, H. T., III, and R. R. Czys (1987). Charge effects on the coalescence of water drops in free fall, Nature, 327, 606–608.

Pawar S.D., D.M. Lal, P. Murugavel (2012), Lightning characteristics over central India during Indian summer monsoon, Atmospheric Research, Volume 106, 44-49,

Pawar S.D., V. Gopalakrishnan, P. Murugavel , N.E. Veremey and A. A. Sinkevich (2017). Possible role of aerosols in the charge structure of isolated thunderstorms, Atmospheric Research 183 463, 331–340.

Peters, G., B. Fischer, H. Münster, M. Clemens, and A. Wagner (2005). Profiles of raindrop size distributions by micro rain radars, *J. Appl. Meteorol*., 44, 1930–1949.

Piepgrass, M. V., E. P. Krider, and C. B. Moore, (1982). Lightning and surface rainfall during Florida thunderstorms, *J. Geophys. Res*., 87, 11, 193- 11, 201.

Price, C., and Federmesser, B. (2006), Lightning-rainfall relationships in Mediterranean winter thunderstorms, *Geophys. Res. Lett.*, 33, L07813, doi:10.1029/2005GL024794.

Pruppacher H.R. and J.D. Klett (1996). *Microphysics of Clouds and Precipitation* (second edition), springer.

Raut, B. A., Konwar, M., Murugavel, P., Kadge, D., Gurnule, D., Sayyed, I., et al. (2021). Microphysical Origin of Raindrop Size Distributions During Indian Monsoon. *Geophysical Research Letters*, 48, e2021GL093581. https://doi.org/10.1029/2021GL093581

Reisner, J., R. M. Rasmussen, and R. T. Bruintjes, (1998). Explicit forecasting of supercooled liquid water in winter storms using the MM5 forecast model. *Quart. J. Roy. Meteor. Soc*., 124, 1071– 1107

Rasmussen, R. M., , and A. J.Heymsfield, (1987b). Melting and shedding of graupel and hail. Part II: Sensitivity study. *J. Atmos. Sci.*, **44**, 2764–2782.

Rogers R. R. and M. K. Yau (1989). *A Short Course in Cloud Physics* (Third edition).

Rosenfeld, D (1999). TRMM observed first direct evidence of smoke from forest fires inhibiting rainfall. *Geophysical Research Letters*, 26(20):3105–3108. ISSN 00948276. doi: 10.1029/1999GL006066.

Rosenfeld D, U. Lohmann, G. B. Raga, C. D. O'Dowd, M. Kulmala, S. Fuzzi, A. Reissell, and M. O. Andreae (2008). Flood or drought: How do aerosols affect precipitation? *Science*, 321, 1309–1313, doi:10.1126/science.1160606.

Rutledge, S. A., and P. V. Hobbs (1983). The mesoscale and microscale structure of organization of clouds and precipitation in midlatitude cyclones. VIII: A model for the ''seeder-feeder'' process in warm-frontal rainbands. J. Atmos. Sci., 40, 1185–1206.

Ryzhkov, A. V., Kumjian, M. R., Ganson, S. M., & Khain, A. P. (2013). Polarimetric Radar Characteristics of Melting Hail. Part I: Theoretical Simulations Using Spectral Microphysical Modeling, *Journal of Applied Meteorology and Climatology*, *52*(12), 2849-2870

Schlamp, R. J., S. N. Grover, and H. R. Pruppachcr, (1976). A numerical investigation of the effects of electric charge and vertical external electric fields on the collision efficiency of cloud drops, J. Atmos. Sci., 33, 1747-1755.

Snook, N., and Xue, M. (2008), Effects of microphysical drop size distribution on tornadogenesis in supercell thunderstorms, *Geophys. Res. Lett.*, 35, L24803, doi:10.1029/2008GL035866.

Srivastava, R. C., (1985). A simple model of evaporatively driven downdraft: Application to microburst downdraft.*J. Atmos. Sci.*, **42 ,** 1004–1023.

Srivastava, R. C. (1987). A model of intense downdrafts driven by the melting and evaporation of precipitation. *J. Atmos. Sci.*, **44 ,** 1752–1774.

Steiner, M., , J. A. Smith, , and R. Uijlenhoet (2004). A microphysical interpretation of radar reflectivity–rain-rate relationships. *J. Atmos. Sci.*, **61 ,** 1114–1131.

Sun L, Qie XS, Mansell ER et al (2018) Feedback effect of electric field force on electrification and charge structure in thunderstorm. Acta Phys Sin 67(16):169201–169201

Takahashi, T., (1978). Riming electrification as a charge generation mechanism in thunderstorms. *J. Atmos. Sci*., 35, 1536–1548.

Takahashi, T. (1984). Thunderstorm electrification- A numerical study, J. *Atmos. Sci*., 41, 2541-2558.

Tao, W. K., Chen, J. P., Li, Z., Wang, C., and Zhang, C (2012). Impact of aerosols on convective clouds and precipitation. *Reviews of Geophysics*, 50(2). ISSN 87551209. doi: 10.1029/2011RG000369.

Tao, W.-K., and Li, X. (2016). The relationship between latent heating, vertical velocity, and precipitation processes: The impact of aerosols on precipitation in organized deep convective systems, *J. Geophys. Res. Atmos.*, 121, 6299– 6320, doi:10.1002/2015JD024267.

Tokay, A., & Short, D. A. (1996). Evidence from Tropical Raindrop Spectra of the Origin of Rain from Stratiform versus Convective Clouds, *Journal of Applied Meteorology and Climatology*, *35*(3), 355-371

Tyagi, A. (2007), Thunderstorm climatology over Indian region. *Mausam*, 58, 189–212.

Virts, K. S., and R. A. Houze Jr. (2015). Variation of lightning and convective rain fraction in mesoscale convective systems of the MJO. *J. Atmos. Sci*., 72, 1932–1944, doi:10.1175/JAS-D-14-0201.1

Waldvogel, A. (1974). The N0 Jump of Raindrop Spectra, *Journal of Atmospheric Sciences*, *31*(4), 1067-1078.

Williams, E. R., and R. M. Lhermitte (1983). Radar tests of the precipitation hypothesis for thunderstorm electrification, *J. Geophys. Res*., 88, 10,984-10,992.

Williams, E. R., S. A. Rutledge, S. C. Geotis, N. Renno, E. Rasmussen, and T. Rickenbach (1992). A radar and electrical study of tropical hot towers, *J. Atmos. Sci*., 49, 1386–1395.

Williams, E. R., & Renno, N. O. (1993). An analysis of the conditional instability of the tropical atmosphere. *Monthly Weather Review*, **121**(1), 21– 36. https://doi.org/10.1175/1520-0493(1993)121<0021:AAOTCI>2.0.CO;2

Williams, E. R. (2005). Lightning and climate: A review, *Atmos. Res*., 76, 272–287.

Williams E.R. (2001). The Electrification of Severe Storms. In: Doswell C.A. (eds) Severe Convective Storms. *Meteorological Monographs. American Meteorological Society*, Boston, MA. https://doi.org/10.1007/978-1-935704-06-5_13.

Williams, E. R., and Co-authors (2010). Ground-based detection of sprites and their parent lightning flashes over Africa during the 2006 AMMA campaign. *Quart. J. Roy. Meteor. Soc*., **136**, 257–271, doi:https://doi.org/10.1002/qj.489.

Winn, W. P., G. W. Schwede, and C. B. Moore (1974). Measurements of electric fields in thunderclouds, *J. Geophys. Res*., 79, 1761– 1767.

Zhang, G., Xue, M., Cao, Q., & Dawson, D. (2008). Diagnosing the Intercept Parameter for Exponential Raindrop Size Distribution Based on Video Disdrometer Observations: Model Development, *Journal of Applied Meteorology and Climatology*, *47*(11), 2983-2992

Zhang, G., J. Sun, and E. A. Brandes (2008). Improving parameterization of rain microphysics with disdrometer and radar observations. *J. Atmos. Sci.,* **63 ,** 1273–1290.

Zhang, H., Zhang, Y., He, H., Xie, Y., & Zeng, Q. (2017). Comparison of Raindrop Size Distributions in a Midlatitude Continental Squall Line during Different Stages as Measured by Parsivel over East China, *Journal of Applied Meteorology and Climatology*, *56*(7), 2097-2111

Figure Captions

Figure 1: (a) Depiction of topographical map of the High Altitude Cloud Physics Laboratory (HACPL), Mahabaleshwar, (India; 17.92 N, 73.66 E) and Atmospheric Electricity Observatory (AEO) at Pune, (India; 18.53N, 73.80E). (b) Nested model domain.

Figure 2: (a-b) Height Time Index (HTI) of radar reflectivity factor (dBZ) for the rain events observed over the High Altitude Cloud Physics Laboratory (HACPL), Mahabaleshwar on 13May, 2015 (SE) and 04 October, 2014 (WE) respectively. The presence of melting layer can be observed at mean sea level (msl) height of 4.6 km. (c-d) surface rain rates (mm hr^{-1}) measured by JW disdrometer. (e-f) Mass weighted diameter (MWD) of raindrops measured (mm) by JW disdrometer. (g-h) Rain intercept parameter, N_0 derived from JW disdrometer using methods of moments following Konwar et al., (2014).

Figure 3: Scatter plot of total lightning (intracloud+cloud-to-ground) observed by the Maharashtra lightning location network (MLLN) on 13 May 2015 near the HACPL.

Figure 4: (a) Scatter plot of N_0 (m^{-3} mm^{-1}) vs. rainwater content W (gm m^{-3}) for strongly electrified (SE) events (indicated by blue stars) observed at the High Altitude Cloud Physics Laboratory (HACPL). The values of N_0 and W are calculated from JW disdrometer measurements using moments method following Konwar et al., (2014). The red line is the best-fit line using the least squares method. The superimposed red dots correspond to the events on 13

May, 2015 (SE) and the black dots correspond to the events on 04 October, 2014 (WE). (b) Bar plot representation of values of N_0 for some SE and WE events observed at the HACPL. The x coordinate indicates number of storms.

Figure 5: Rain evaporation rate (kg kg^{-1} s^{-1}) for the events shown in Figure 2(a-b). The evaporation rate is calculated by using equation (1) from the microrain radar (MRR) measured values of raindrop size distribution parameters. The vertical resolution of MRR measurement is 300m. SE and WE indicate strongly and weakly electrified events, respectively. The height is measured from mean sea level (msl). The msl height of the HACPL is 1.3 km. Data from the lowest measuring height (1.6km) is discarded.

Figure 6: Bar graph representation of N_0 (m^{-3} mm^{-1}) vs. surface-measured E field (V m^{-1}) for a few SE events observed for the year 2008 at the Atmospheric Electricity Observatory (AEO) at Pune (a)3rd June, (b) 31 August,(c) 8 September and (d) 9 September. The values of N_0 are grouped in E field bins of width 500 V m^{-1}. Each bar in the plots corresponds to the mean value of the respective bin. (e-h) The corresponding bar graph representation of rain evaporation rates (ER) vs. E field for the same events as shown in (a-d).

Figure 7: Results from the idealized simulations (a) accumulated rain (mm) (b) Evaporation rate (kg kg^{-1} s^{-1}) (c) Maximum vertical velocity (ms^{-1}). The blue curves correspond to the default wsm6 scheme and the green curves correspond to the modified scheme indicated as wsm6(M).

Figure 8: Results from observed case (13 May 2015) simulation (a) Comparison of simulated rain rate to the observed rain rate at the HACPL (mm hr^{-1}). (b) Daily accumulated rain (mm), averaged over a 25km×25km box, with the HACPL being in the middle. IMD indicates Indian Meteorological Department, TRMM indicates the Tropical Rainfall Measuring Mission and JWD indicates JW disdrometer measurements.

Figure 9: Results from observed case simulation (13 May 2015). (a) Height Time Index (HTI) of area-averaged vertical velocity (m s^{-1}) for wsm6 (b) same as (a) but for wsm6(M).

Figure 10: Results from observed case simulation (5 May 2015). (a) Height Time Index (HTI) of area-averaged vertical velocity (m s^{-1}) for wsm6 (b) same as (a) but for wsm6(M).

Figure 11: Schematic representation of the evolution of weakly and strongly electrified storms. In a weakly electrified (WE) storm, the number of smaller raindrops are numerous, the evaporation of which resulted in latent cooling, thereby initiating the downdraft at the mature stage of the storm. In strongly electrified (SE) storms, electrically induced coalescence reduces the number of smaller raindrops and increases the number of larger ones and thereby reducing the latent cooling. The reduction of latent cooling delays the initiation of downdraft. This process acts to provide positive feedback to storm updraft intensity in strongly electrified storms. The length of the arrows indicates the strength of vertical velocity.

Table 1: Results from the two observed strongly electrified (SE) events simulations.

Events	Observed cloud parameters	Control run ($N_0 = 8 \times 10^6\ m^{-4}$) wsm6	Modified run ($N_0 = 1.6 \times 10^6\ m^{-4}$) wsm6(M)	Relative changes
13May, 2015	**CTH=**8.5km **FR**=4flashes min^{-1} **RI=** 4.33 mm hr^{-1} **R**=11.32 mm T= 2 hours	**R**=6.77 mm, **Wmax**= 34.70 ms^{-1} **QI**= 3.87×10^{-4} kg kg^{-1}	**R**= 8.233 mm, **Wmax**= 37.44 ms^{-1} **QI**= 4.21×10^{-4} kg kg^{-1}	% change in R=21%
5 May, 2015	**CTH=**not available **FR**=9 flashes min^{-1} **RI =** 16.42 mm hr^{-1} **R**=11.52 mm T=2 hours	**R**= 2.94mm, **Wmax**=48.01 ms^{-1} **QI**= 2.49×10^{-4} kg kg^{-1}	**R**= 5.18 mm , **Wmax**= 51.52 ms^{-1}, **QI**= 3.14×10^{-4} kg kg^{-1}	% change in R=76%

Note: 'R' indicates area-averaged accumulated rain rate in mm. The observed R values are obtained from the Tropical Rain Measuring Mission (TRMM) 3B-42 precipitation datasets. FR indicates flash rate obtained from Maharashtra Lightning Location Network (MLLN). 'CTH' indicates cloud top height obtained from the Moderate Resolution Imaging Spectroradiometer (MODIS) (Terra platform) collection 6. 'RI' indicates peak rain intensity, 'T' indicates storm life time, 'N_0' is the rain intercept parameter, 'QI' indicate domain-averaged total mass mixing ratio of ice-phase hydrometeors (graupel+ice+snow) and 'Wmax' is the maximum simulated vertical velocity.

1008

1009

1010

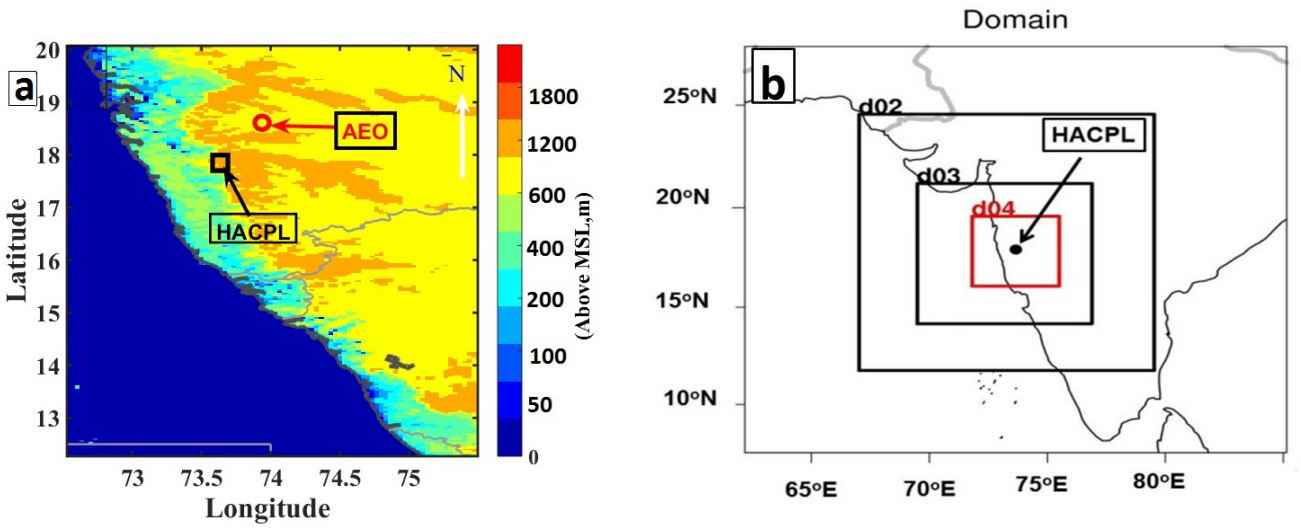

Figure 1: (a) topographical map depicting the High Altitude Cloud Physics Laboratory (HACPL), Mahabaleshwar, (India; 17.92 N, 73.66 E) and Atmospheric Electricity Observatory (AEO) at Pune, (India; 18.53N, 73.80E).(b) Nested model domain

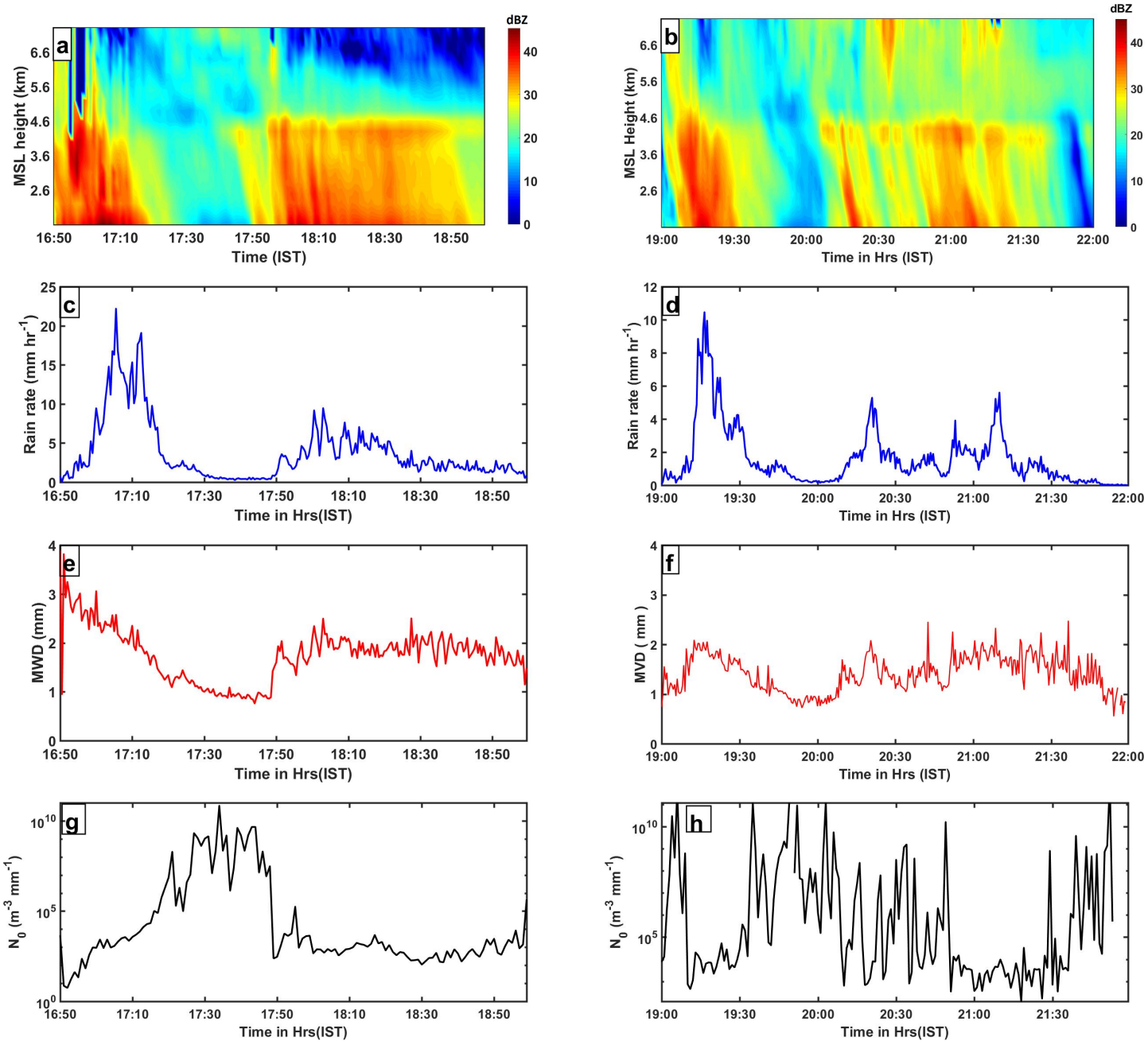

Figure 2: (a-b) Height Time Index (HTI) of radar relectivity factor (dbz) for the rain events observed over the High Altitude Cloud Physics Laboratory (HACPL), Mahabaleshwar on 13May,2015 (SE) and 04 October,2014 (WE) respectively. The presence of melting layer can be observed at msl height of 4.6km. (c-d) surface rain rates(mm hr^{-1}) measured by JW disdrometer, (e-f) Mass weighted diameter (MWD) of raindrops measured(mm) by JW disdrometer.(g-h) Intercept parameter N_{0r} derived from JW disdrometer using momenets methods follwoing Konwar et al., (2014).

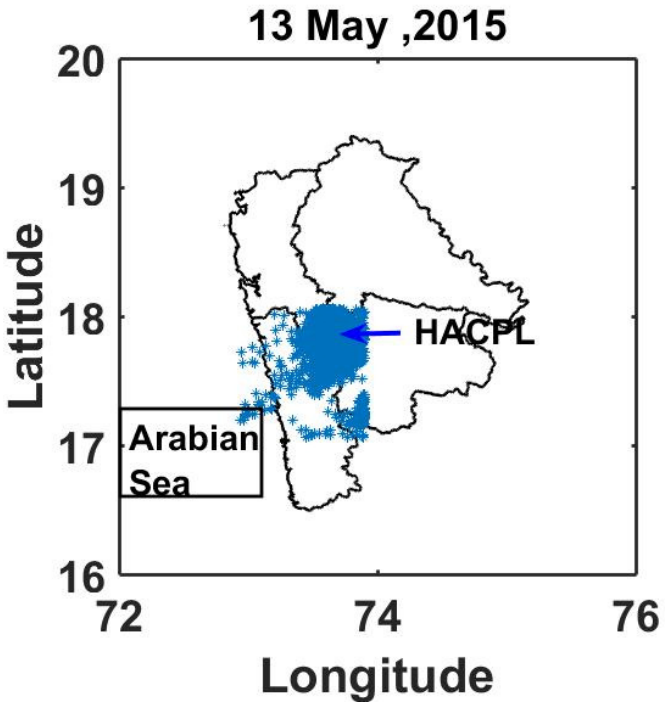

Figure 3: Scatter plot of lightning observed by the Maharashtra lighting location network (MLLN) on 13 May, 2015 near the HACPL.

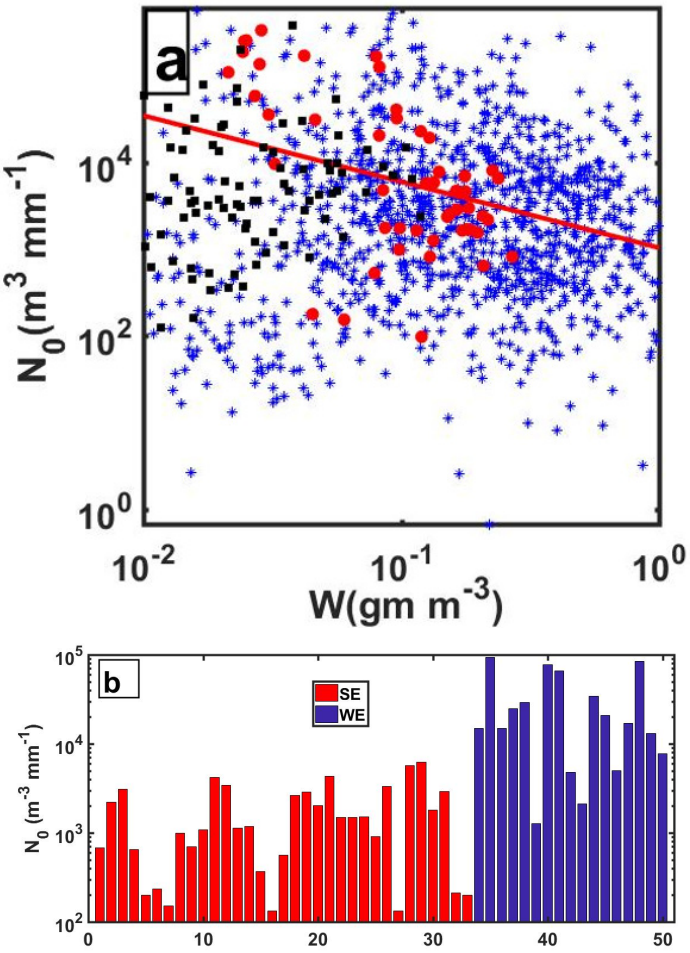

Figure 4: (a) Scatter plot of $N_{0r}(m^{-3}mm^{-1})$ vs rainwater content W (gm m^{-3}) for SE events observed at the High Altitude Cloud Physics Laboratory (HACPL). The values of N_{0r} and W are caluclated from JW disrometer measurements using moments method following Konwar et al., (2014). The red line is the best-fit line using the least sqaures method. The superimposed red dots correponds to the events on 13 May, 2015 (SE) and the black dots correponds to the events on 03 October, 2014 (WE). (b) Bar plot representation of values of N_{0r} for some SE and WE events observed at the HACPL. The

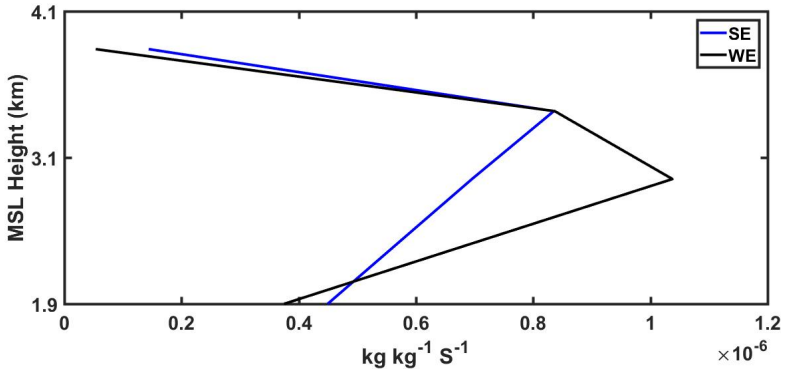

Figure 5: Rain evaporation rate (kg kg$^{-1}s^{-1}$) for the events shown in Figure 2(a-b). The evaportaion rate is calculated by using equation (1) from the microrain radar (MRR) measured values of raindrop size distribution parameters.SE and WE indicate strongly and weakly electrified.

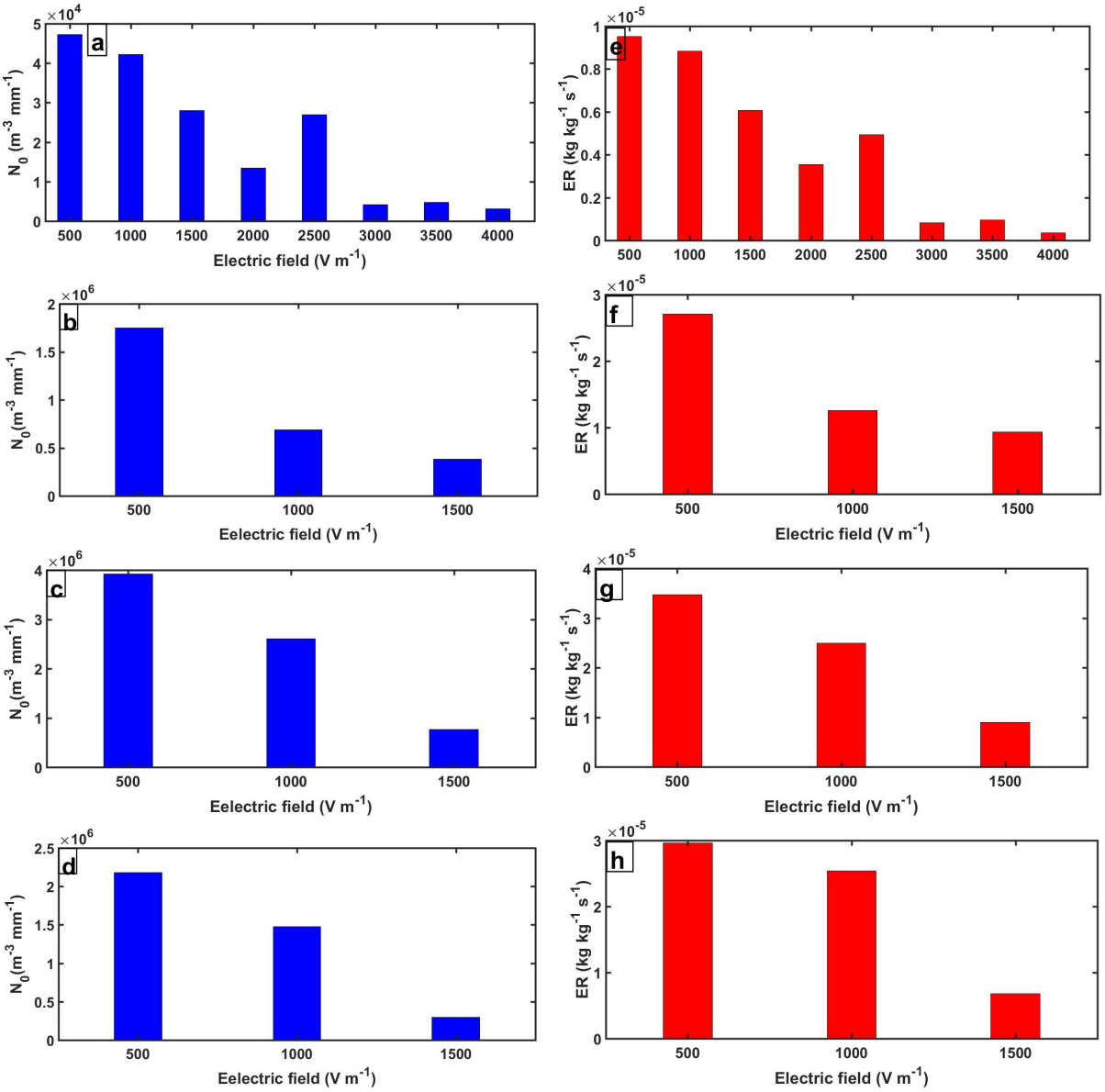

Figure 6: Bar plot of rain intercept parameter, N0 (m^{-3} mm^{-1}) vs. surface measured E field (V m^{-1}) for a few SE events observed for the year 2008 at the Atmospheric Electricity Observatory (AEO) at Pune (a)3rd June, (b) 31 August,(c) 8 September and (d) 9 September. The values of N0 are grouped in E field bin of width 500 V m^{-1}. (e-h) The corresponding bar plot of evaporation rate (ER) vs. E field for the same events as shown in (a-d).

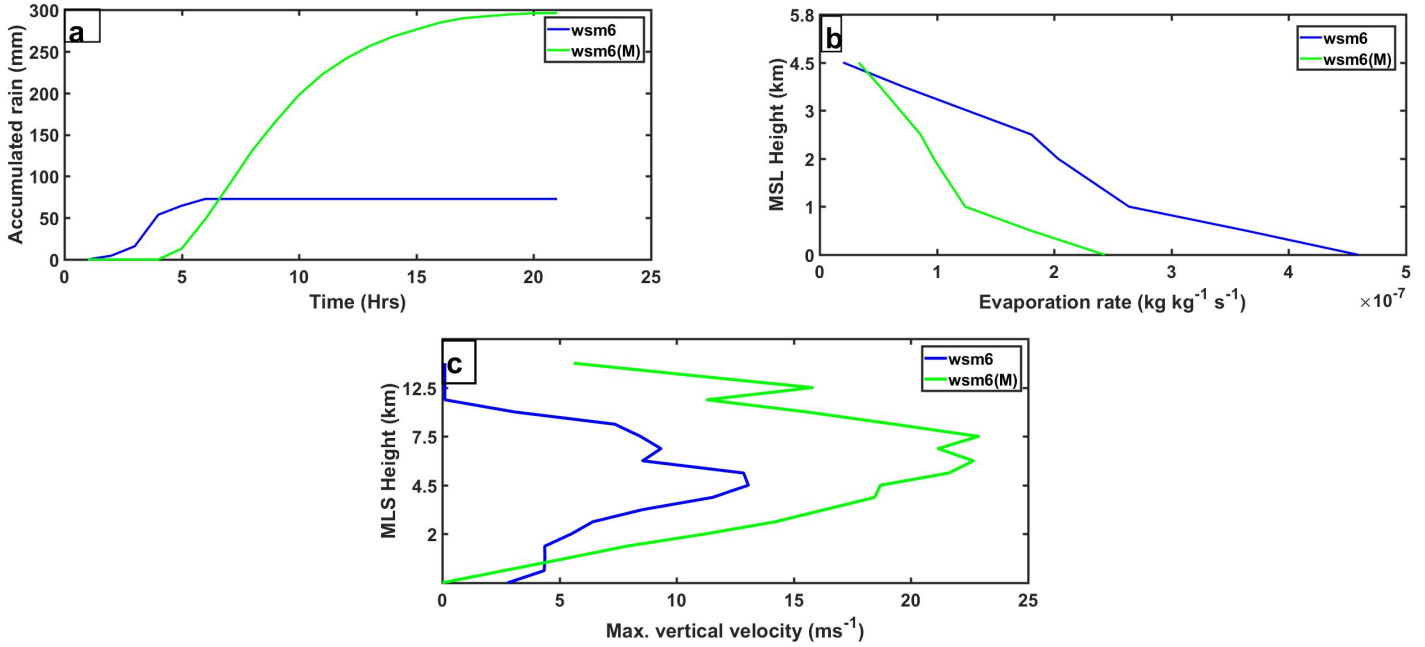

Figure 7: Results from the idelaized simulations (a)accumulated rain (mm) (b) Evaporation rate (kg kg$^{-1}s^{-1}$) (c) Maximum vertical velocity (m s^{-1}). (d) Vertical profiles of ice phase hydrometeors (kg kg^{-1}). The solid curves corresponds to wsm6 scheme and dashed curves corresponds to wsm6(M).

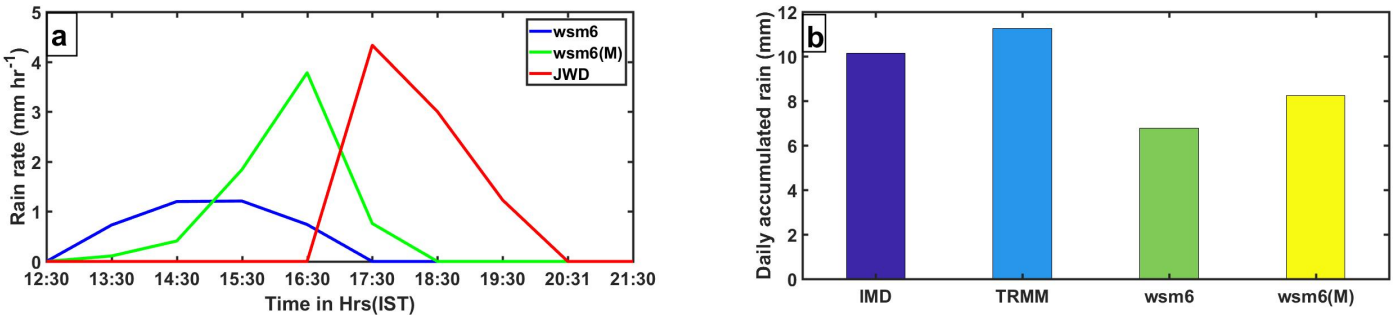

Figure 8: Results from real case (13 May ,2015) simulation (a) Rain rate (mm hr^{-1}).(b) Daily accumulated rain. IMD indicate Indian meteorological department. TRMM indicate the Tropical Rainfall Measuring Mission. (c) Probability Density Function (PDF) for rain .

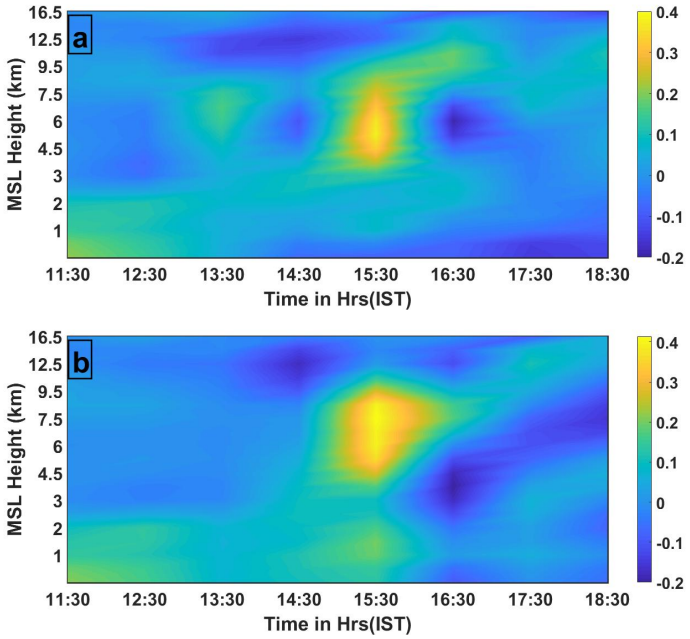

Figure 9: Results from real case simulation (13 May 2015)(a) Height Time Index of area averaged vertical velocity (m s^{-1}) for wsm6 (b) same as (a) but for wsm6(M)

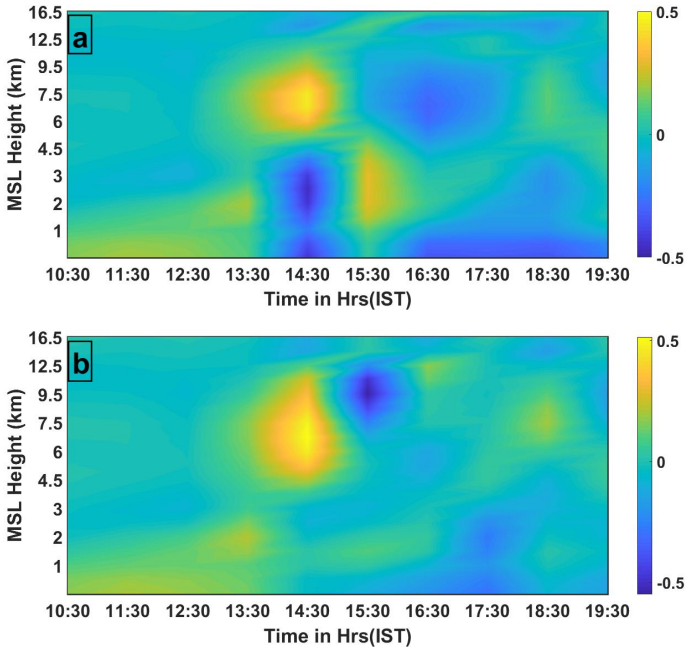

Figure 10: (a) Simulated CAPE for the storm on 13 May, 2015 averaged over a 25km×25km box, the HACPL being in the middle. (b) Total flash count in the said box derived from Maharashtra lightning location network (MLLN) for the storm.

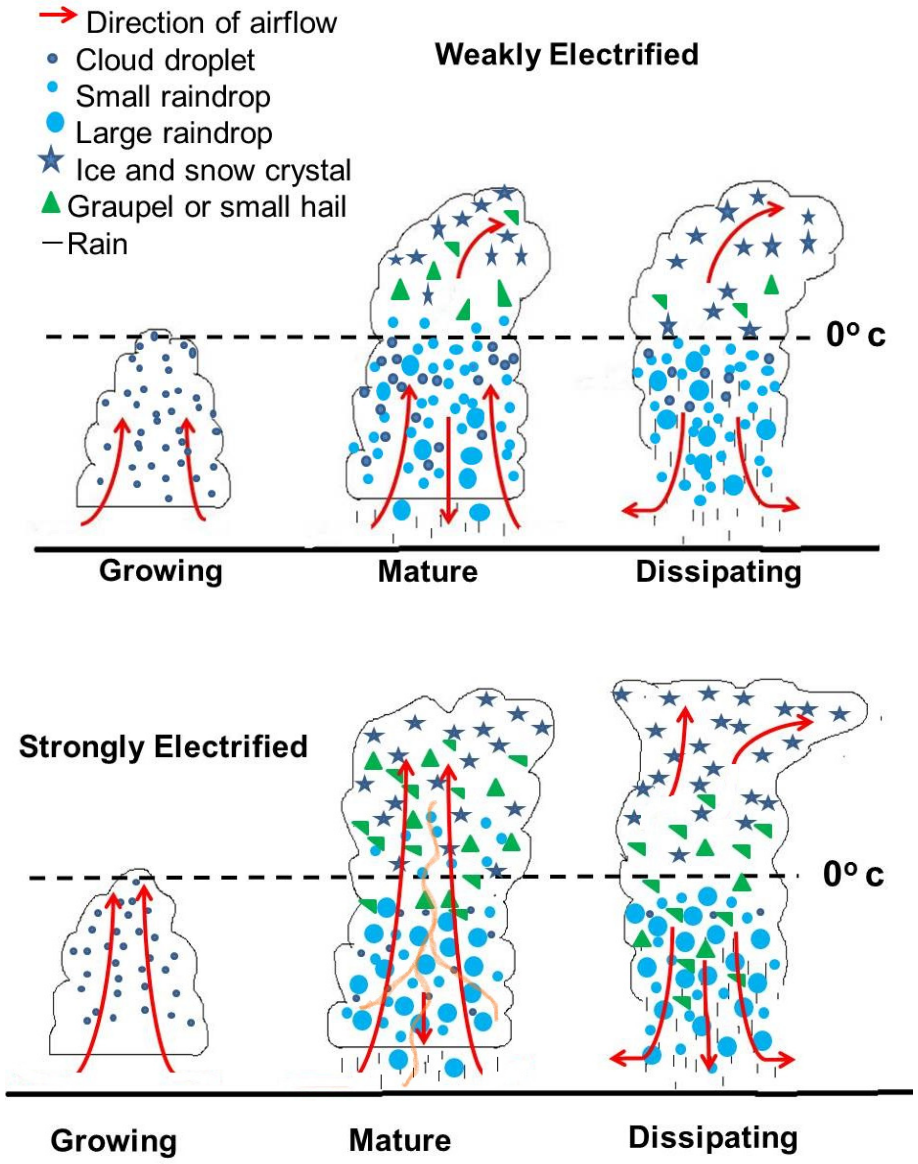

Figure 11: Evolution of weakly and strongly electrified storms. In a weakly electrified storms, number of smaller raindrops are numerous evaporation of which resuted in latent cooling, thereby initiating downdraft at the mature stage of the storm. In strongly electrified storms, electrically induced coalesence reduces the number of smaller raindrops and increase the number of larger ones and thereby reduces the latent cooling. This delays the intiation of downdraft. This process acts to provide a positive feedback to storm updraft intensity in strongly electrified storms. The length of the arrows indicate strenght of vertical velocity.